crystals

MDPI

Review

Review on the Corrosion Behaviour of Nickel-Based Alloys in Supercritical Carbon Dioxide under High Temperature and Pressure

Yiyao Kang, Xuesong Leng *, Lin Zhao, Bowen Bai, Xiaoya Wang and Hongsheng Chen *

Institute of Special Environments Physical Sciences, Harbin Institute of Technology (Shenzhen), Shenzhen 518055, China

* Correspondence: lengxuesong@hit.edu.cn (X.L.); chenhongsheng@hit.edu.cn (H.C.)

Abstract: Supercritical carbon dioxide (S-CO_2) has the advantages of amphoteric liquid and gas, which possesses many unique characteristics, such as good compressibility, high density, high solubility, good fluidity and low viscosity. The Brayton cycle with S-CO_2 is considered to have many promising applications, especially for power conversion industries. However, the corrosion and degradation of structural materials hinder the development and application of the Brayton cycle with S-CO_2. Nickel-based alloys have the best corrosion resistance in S-CO_2 environments compared to austenitic stainless steels and ferritic/martensitic steels. Thus, the present article mainly reviews the corrosion behaviour of nickel-based alloys in S-CO_2 under high temperature and pressure. The effect of alloying elements and environment parameters on the corrosion behaviour of different nickel-based alloys are systematically summarized. The conclusion and outlook are given at the end.

Keywords: supercritical carbon dioxide; corrosion behaviour; nickel-based alloys; oxidation; carburization

check for updates

Citation: Kang, Y.; Leng, X.; Zhao, L.; Bai, B.; Wang, X.; Chen, H. Review on the Corrosion Behaviour of Nickel-Based Alloys in Supercritical Carbon Dioxide under High Temperature and Pressure. *Crystals* **2023**, *13*, 725. https://doi.org/10.3390/cryst13050725

Academic Editors: Marzena Mitoraj-Królikowska, Marcela E. Trybula and James L. Smialek

Received: 19 March 2023
Revised: 20 April 2023
Accepted: 20 April 2023
Published: 25 April 2023

Copyright: © 2023 by the authors. Licensee MDPI, Basel, Switzerland. This article is an open access article distributed under the terms and conditions of the Creative Commons Attribution (CC BY) license (https://creativecommons.org/licenses/by/4.0/).

1. Introduction

The fluids in environments above critical temperature and pressure are called supercritical fluids [1]. Supercritical carbon dioxide (S-CO_2), whose critical point is 31.1 °C and 7.38 MPa, has the advantages of amphoteric liquid and gas, such as the characteristics of high density and solubility, which is similar to the liquid, and low viscosity, which is similar to the gas [2,3]. S-CO_2 possesses many unique characteristics, such as good compressibility, high density, high solubility, good fluidity and low velocity [4]. Therefore, it can be used in many applications such as extraction, power conversion, and refrigeration. The Brayton cycle, which uses S-CO_2 as the medium to transfer heat, is considered to be potentially significant for power conversion due to its high efficiency, lower cost, lower noise, nontoxicity, high stability and a compact structure [5]. The Brayton cycle can be used in many applications, such as the power conversion for the Generation IV nuclear reactor [6], thermal power systems [7], solar power systems [8] and other systems.

The Brayton cycle consists of at least five components: heater, turbine, precooler, compressor and working fluid. It is a thermal cycle system composed of four processes: adiabatic compression, isobaric heating, adiabatic expansion and isobaric cooling [9]. Today, the Brayton cycle with S-CO_2 has aroused great interest, and many researchers have investigated the Brayton cycle with S-CO_2 from many aspects, including the key factors and components, the method to increase the thermal efficiency and thermodynamics [9–11]. Although extensive studies have been carried out, there are still some problems that have not been fully resolved. One of the most urgent problems is the corrosion and degradation of structural materials caused by the harsh working conditions of high temperature and pressure, which hinders the implementation and commercialization of the Brayton cycle with S-CO_2 [12]. Generally speaking, the test system of corrosion behaviour for metallic materials in the Brayton cycle should include the following parts: gas supply system,

high pressure CO_2 pumping system, CO_2 preheater, temperature- and pressure-controlled autoclave, CO_2 precooler, gas sampling and analysis system and computer systems for process control and data acquisition. This system can control the temperature rise rate, pressure boost rate, CO_2 velocity and other parameters related to the corrosion experiments.

Preliminary research results show that the corrosion resistance of different materials vary greatly in S-CO_2 environments. In general, nickel-based alloys have slightly better corrosion resistance than austenitic stainless steels, and austenitic stainless steels have significantly better corrosion resistance than ferritic/martensitic steels [10–15]. The ferritic/martensitic steels and austenitic stainless steels cannot fully meet the requirements of core structural materials required by the Brayton cycle with S-CO_2. In contrast, nickel-based alloys can better adapt to the harsh working conditions in the Brayton cycle with S-CO_2. Therefore, on the basis of reviews of corrosion behaviour of alloys in high-temperature and -pressure S-CO_2 environments [15,16], the present article mainly reviews the corrosion mechanism of structural materials, emphasizing the corrosion behaviour of nickel-based alloys in S-CO_2 environments under high-temperature and -pressure conditions.

2. Corrosion Mechanism

First, the corrosion mechanism of alloys in high-temperature and -pressure S-CO_2 environments should be clarified. At present, many studies have conducted research on the corrosion mechanism of metallic materials in S-CO_2 environments, mainly exploring the corrosion reaction processes of metallic materials and the composition of corrosion products of different metallic materials and comparing the corrosion resistance of different metallic materials in S-CO_2 environments.

2.1. Corrosion Reaction Processes

For structural materials, both oxidation and carburization will occur in high- temperature and -pressure S-CO_2. In this section, the mechanisms of oxidation and carburization of metallic materials in S-CO_2 and the corrosion behaviour of various structural materials in S-CO_2 will be described briefly.

2.1.1. Oxidation

In S-CO_2, CO_2 produces a partial pressure of oxygen, which is sufficient to oxidize alloying elements such as Fe and Cr. Thus, oxidation will occur between the oxygen, which is formed by the decomposition of CO_2, and the alloying elements. The oxygen reactions are described by Reactions (1) and (2) [13]:

$$xM + yCO_2 \rightarrow M_xO_y + yCO \quad (1)$$

$$xM + \frac{y}{2}CO_2 \rightarrow M_xO_y + \frac{y}{2}C \quad (2)$$

where M represents alloying elements such as Cr and Fe. With the formation and amassment of oxide on the surface, the corrosion resistance is determined. A Cr-rich oxide layer usually shows better corrosion resistance than the Fe-rich oxide. The higher corrosion resistance of the Cr-rich oxide layer is mainly attributed to the continuous and dense layer, which will play a protective role in curbing further oxidation. In contrast, the discontinuous and porous Fe-rich layer provides a channel for the permeation and diffusion of the corrosive gases into the matrix and triggers further oxidation of the sublayer matrix.

Researchers have also calculated the rate of oxidation by measuring weight gains, which are related to the constant K_w, and oxide thickness, which is related to the constant K_p [17]. The two constants are both parabolic constant. The smaller the constants are, the better the corrosion resistance of the alloys. The method of calculating the constants is given by Reactions (3) and (4) [2,18]:

$$K_\omega = \frac{\Delta\omega}{t^n} \quad (3)$$

$$K_p = \frac{X^2}{2t} \quad (4)$$

where $\Delta\omega$ stands for the weight gains, n means the time exponent that describes the time dependence of the oxide growth, X represents the thickness of the oxide layer and t is time. Figure 1 shows the corrosion kinetics of typical alloys in high-temperature CO_2; all alloys follow the parabolic law [13].

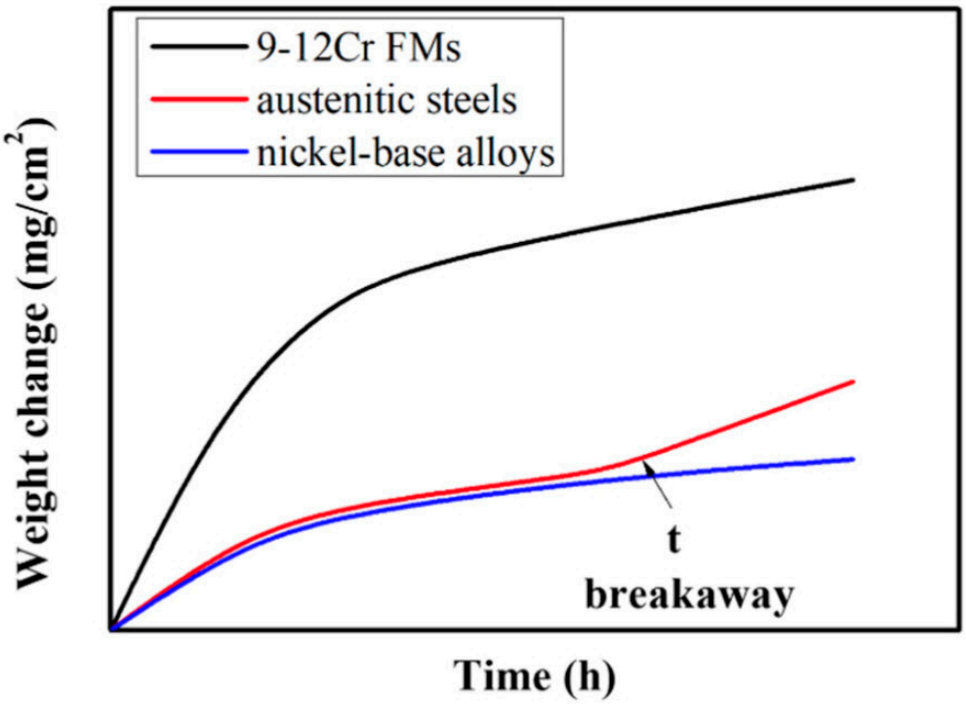

Figure 1. The corrosion kinetics of typical alloys in high−temperature CO_2. Reprinted from [16] under Creative Commons Attribution (CC BY) license.

Researchers also conducted experiments on the mechanism of oxidation [19–23]. It is proved that the occurrence of oxidation is controlled by ion diffusion, and the driving force of diffusion is mainly the concentration differences of chemical substances and components [19–21]. In addition, the concentration differences in chemical substances and components will lead to different oxygen activity across the oxide layer, which ultimately drives the oxidation. It is also proved that CO_2 can induce the growth of an oxide layer by providing oxygen partial pressure higher than required for the formation of the oxide layer [22].

2.1.2. Carburization

The carburization process consists of two main steps. First, the gas that contains carbon permeates through the oxide layer on the surface of the alloys. Subsequently, some of the C combines with some alloying elements to form a carbide precipitate, while another part forms an amorphous carbon layer at the interface between the oxide layer and the matrix [24]. Scholars have different understandings about the origin of C, and the conclusions drawn by scholars also have distinctions. However, the conclusions are basically thermodynamically equivalent [25,26]. The most well-known reaction of C generation is called the Boudouard reaction, as presented in Reactions (5) and (6) [22,23,27]:

$$2CO_2 \leftrightharpoons 2CO + O_2 \quad (5)$$

$$2CO \leftrightharpoons CO_2 + C \quad (6)$$

Some researchers suggest that in addition to the Boudouard reaction, the direct decomposition of CO or CO_2 will also lead to the production of C [4,28].

However, the activity of C is quite low in high-temperature CO_2 at atmospheric pressure [22,23]. Thus, it is necessary to explain why carburization occurs under high pressure. This is because the area where carburization occurs is not in direct contact with ambient CO_2 but instead within the inner layer of the oxide layer, which causes the distinction of oxygen activity. The oxygen activity at the oxide layer surface is equal to the CO_2 dissociation pressure, while it is equal to the oxide dissociation pressure at the interface between the oxide layer and the matrix. The activity of C is inversely proportional to the activity of oxygen according to the equilibrium constant of Reactions (5) and (6). Therefore, the C activity at the interface between the oxide layer and the matrix is high enough to induce a carburization reaction [15,17,22,23].

2.2. Corrosion Behaviour and Resistance of Different Metallic Materials

At present, there are three main categories of alloys used in the S-CO_2 Brayton cycle, namely ferritic/martensitic steel, austenitic stainless steel and nickel-based alloy. This section mainly introduces their corrosion behaviour and corrosion resistance in high-temperature and -pressure S-CO_2.

For the corrosion behaviour of both ferritic/martensitic steels and austenitic stainless steels such as 12Cr and 316, oxidation reactions will occur in S-CO_2 environments, in which the outer layer is Fe_3O_4 with coarse columnar grains and the inner layer is $Fe(Fe_{1-x}Cr_x)2O_4$, which is made of small equiaxed grains.

For ferritic/martensitic steels, F. Rouillard [13] and L. Tan [14] both have reported the corrosion behaviour of 9–12Cr ferritic/martensitic steel, which forms a duplex oxide layer that includes coarse columnar Fe_3O_4 magnetite grains covered by small equiaxed Fe_2O_3 hematite grains as the outer layer and a complex mixture of nano- to micro-sized $Fe_{3-x}Cr_xO_4$ spinel oxide grains with some nonoxidized carbides as the inner layer. However, with the increasing chromium content of ferritic/martensitic steels, a thin and protective chromia layer will be formed, and the oxide rate will be slowed down [23,29].

Austenitic stainless steels, which can rapidly form a protective chromia layer on the surface of the matrix, exhibit higher corrosion resistance than ferritic/martensitic steel in S-CO_2 environments with temperatures higher than 550 °C [19,23,30]. However, many carbides were observed under the oxide layer, which is caused by carburization [14]. The carbon that reacts with the carbide-forming elements comes from molecules such as CO and CO_2, which reach the interface between the oxide layer and the matrix through grain boundaries, microchannels and nanopores in the oxide layer. Among these carbides are Cr-rich, Nb-rich, V-rich, Fe-rich and W-rich, depending on the composition of the steel. In addition, the carbides mainly present in fine intragranular and intergranular form. The presence of these carbides will lead to the deterioration of corrosion resistance by pinning the movements of Cr [17]. Due to the austenitic structure having a lower diffusion coefficient, larger growth stress and thermal stress during oxidation, spallation will occur occasionally. This will cause the oxidation layer to lose protection, increasing the consumption of Cr by exposing Cr in the matrix to the ambient gases and thus finally resulting in a severe Cr-depletion zone [31].

Moreover, the corrosion conduct as with Fe_2O_3 has the photoelectric properties of a semiconductor [17]. Thus, under illumination, the corrosion product will generate electrons and holes, which can be directly involved in the electrochemical process of matrix corrosion and may accelerate the corrosion rate [23].

Nickel-based alloys have the greatest corrosion resistance compared to ferritic/martensitic steels and austenitic stainless steels [32,33]. Their specific corrosion behaviour, corrosion resistance and effect factors are introduced in detail below.

2.3. Summary

This section mainly introduces the mechanisms of oxidation and carburization and the corrosion behaviour of typical alloys in high-temperature and -pressure S-CO_2. The main purpose is to give the reader a brief understanding of the corrosion process in S-CO_2 environments.

Next, the factors affecting the corrosion behaviour of nickel-based alloys are introduced. Many factors can affect the corrosion behaviour of nickel-based alloy in high-temperature and -pressure S-CO_2 environments. In essence, the factors can be divided into two categories:

1. Factors associated with the alloying elements, such as chromium, molybdenum, tungsten, niobium and so on;
2. Parameters related to the corrosion environment of nickel-based alloy such as temperature, pressure, impurities and flow rate.

3. Factors Associated with the Alloying Elements

For nickel-based alloys, many metallic elements are used as the alloying elements such as chromium, cobalt, molybdenum, titanium, silicon, manganese and aluminum. However, by adding different alloying elements, the corrosion resistance of nickel-based alloys will also change. Thus, this section introduces the factors that are associated with the alloying elements, which will affect the corrosion behaviour of nickel-based alloys in high-temperature and -pressure S-CO_2 environments.

3.1. Major Elements

For nickel-based alloys, the major elements generally include nickel, iron and chromium. Among them, as matrix elements, iron and nickel have the higher content. In addition, as the most important element for providing corrosion resistance for nickel-based alloys, the content of chromium is usually more than 15%.

3.1.1. Effect of Fe and Ni Content

For Ni-based alloys, the different content of Fe and Ni will lead to a distinction in some of the corrosion product. However, with the formation of the continuous and protective chromia layer, the distinction has a minor effect on the oxidation resistance of the alloys. In addition, the faster diffusion rate of C in Fe than in Ni will deteriorate the carburization resistance at lower temperatures, while the rate of carbon uptake may be independent of the content of Fe and Ni at higher temperatures.

Alloy 800 is a relatively nickel-based alloy series that contains iron, nickel and chromium with trace amounts of manganese, aluminum and titanium. The corrosion behaviour and resistance of its variants (Alloy 800, 800H and 800HT) are widely studied by many researchers [14,24,34–36]. They all pointed out in their studies that Alloy 800 variants have great corrosion resistance in high-temperature and -pressure S-CO_2 environments, which is mainly attributed to the thin and uniform chromia layer. The oxidation rate follows the parabolic law ($\Delta W = K_P\sqrt{t}$), which suggests that the oxidation is a diffusion-controlled process. Moreover, according to G. Cao's research [35], a multiple stoichiometric oxide layer, including Cr_2O_3, $Cr_{1.4}Fe_{0.7}O_3$, $FeCr_2O_4$, $Ni_{1.4}Fe_{1.7}O_4$, $FeMn_2O_4$ and Al_2O_3, was formed for Alloy 800H, which provides superior corrosion resistance. This also reflects that for Alloy 800 variants, the oxidation resistance is almost equivalent to ordinary nickel alloys.

As for carburization resistance, researchers have also conducted studies. Benjamin Adam mainly studied the carburization behaviour of Alloy 800H [36]. It was found that high-temperature and -pressure S-CO_2 environments have an evident effect on carburization behaviour, the Cr depletion zone and the recrystallization zone of Alloy 800. He lists three main reason to explain this phenomenon, which are the stresses generated with the formation of the oxide layer, the increase of grain boundary density and the availability of monatomic carbon.

Ho Jung Lee et al. [37] characterized the carburization of Alloy 600, Alloy 690 and Alloy 800HT. A layer of amorphous C, which represents the carburization, is observed below the oxide layer. In addition, the oxide layer is continuous without any spallation. This means that the chromium content has little effect on carburization resistance because the chromia layer remains continuous. Some Cr-rich M_6C_{23} carbides were observed under the amorphous C layer for only Alloy 800HT, which suggests that Alloy 800HT has worse carburization resistance than Alloy 600 and Alloy 690. For the tested alloys, Alloy 800HT is an iron-nickel-based alloy, while Alloy 600 and Alloy 690 are nickel-based alloys. Therefore, from the perspective of the different matrices, the lower activity of chromium in nickel and the lower solubility and diffusion coefficient of C in iron lead to the distinction for carburization resistance.

However, a recent experiment has also shown that the effect of carburization on Fe and Ni content may be less pronounced than previously thought, at least at higher temperatures. Oleksak et al. [38] tested several Ni-based alloys at 700 °C for 10,000 h. The results show that Alloy 800 has a carbon uptake similar with Ni-based alloys, which suggests that the rate of carbon uptake is independent of the Fe/Ni ratio.

Through analysis of the above experimental results, the effect of Fe and Ni can be concluded. For oxidation, the resistance of nickel-based alloys and iron-nickel-based alloys in S-CO_2 is superior, which is attributed to the high content of Ni which can accelerate the formation of protective chromia and inhibit the further thickening of the oxide layer [39]. As for carburization, it is suggested that the resistance of the alloys with higher Fe content is poorer at lower temperature. This is because Ni has a higher solubility than Fe, and thus Ni-based alloys can provide higher carburization resistance by reducing the precipitation of carbides [40,41]. In addition, at higher temperatures, the carburization resistance may be independent of the content of Fe and Ni.

3.1.2. Effect of Cr Content

The content of Cr plays a crucial role in corrosion resistance. When the content of Cr is sufficient, the Cr will tend to react with oxygen and form a continuous and protective chromia layer to prevent further oxidation and carburization.

Thus, Cr is the most important element that makes the alloy have good corrosion resistance in high-temperature and -pressure S-CO_2 environments. Cr can form a continuous thin-layer chromia with superior stability and protectiveness. Higher Cr content makes the alloy more inclined to form chromia films in the corrosion to obtain oxidation and carburization resistance [42]. For nickel-based alloys, it is suggested that the Cr content of at least 14% is required to form a protective chromia layer [43].

Even if the content of Cr reaches the critical point and forms a continuous chromia layer, oxidation and carburization may still happen. This is because C tcan penetrate through the chromia layer and form an amorphous C layer between the matrix and the chromia, which leads to carburization. Then, after the formation of amorphous C, spallation of the oxide layer may be triggered and results in further oxidation.

Experiments also confirmed the theory above. Xianglong Guo et al. [43] tested the long-term oxidation and carburization mechanism of Alloy 800H at 650 °C and 20MPa for 3000 h. Although Alloy 800H has a relatively high content of Cr, spallation still happened after 2000 h, which is shown in Figure 2. The inner $MnCr_2O_4$, the SiO_2 layer and the amorphous C can be observed. This is believed to promote spallation. Oleksak [44] also suggests that only when the content of Cr is sufficient, which is about 22%, will its content not affect the oxidation rate.

In general, for nickel-based alloy, a 14% content of Cr is enough to form a continuous chromia layer. However, further oxidation and carburization may still occur. Thus, as a candidate structural material for the Brayton cycle, it is best to increase the content of Cr to more than 22% to resist corrosion as much as possible.

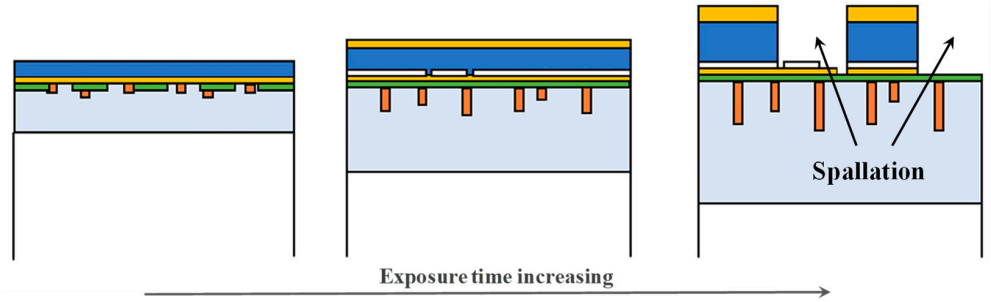

Figure 2. Schematic illustration of spallation for Alloy 800. Yellow layer stands for $MnCr_2O_4$. Blue layer stands for the Cr_2O_3. White layer stands for the amorphous C. Green layer stands for the SiO_2. Orange layer stands for the Al_2O_3. Grey area stands for the Cr-depletion region. Reprinted from Xianglong Guo, Zhu Liu, Ling Li, Jichang Cheng, Haozhan Su, and Lefu Zhang. "Revealing the long-term oxidation and carburization mechanism of 310S SS and Alloy 800H exposed to supercritical carbon dioxide." Materials Characterization 183 (2022): 111603. Copyright 2021, with permission from Elsevier [43].

3.2. Trace Elements

Nickel-based alloys, as a candidate structural material for Brayton cycle, should serve in harsh working conditions. Higher requirements are needed for the high-temperature performance of nickel-based alloys. To improve the hardness of the alloy, molybdenum and niobium are added as solid-solution elements. To improve the long-term performance, cobalt, titanium, aluminum and silicon are needed. Therefore, with the addition of these alloying elements, it is important to discuss their effects on corrosion resistance.

3.2.1. Effect of Co Content

According to a few existing studies, it can be roughly concluded that increasing the content of Co is beneficial for improving the carburization resistance of Ni-alloys. A relatively higher content of Co is beneficial for the carburization resistance and high-temperature properties of alloys, according to J.R. Davis [45]. However, for the effect of Co content on the corrosion resistance of nickel-based alloys, only a few studies have been done. One study about Alloy 188 has been made at 700–1000 °C and 20 MPa S-CO_2. Alloy 188 is a kind of Co-based alloy. It is suggested that it has great corrosion resistance, and no carburization was observed [46]. Based on the results above, it can be inferred that the addition of Co can improve the carburization resistance of nickel-based alloys. Research on the carburization resistance of high Co content (Alloy 617) also proved the inference [30]. However, one study suggests the opposite [38]. Alloy 617 shows the poorest carburization resistance compared to several Ni-based alloys. Thus, in order to clarify the effect of the Co, more research should be done.

3.2.2. Effect of Ti Content

Ti tends to be oxidized into TiO_2, which can decrease in corrosion rate as an underlying sublayer or precipitate in the internal oxidation zone. However, Ti may also cause the increase of the cation to diffuse along the grain boundary and effect corrosion resistance.

As an alloying element, Ti is usually used in most heat- and corrosion-resistant nickel-based alloys and will be oxidized into TiO_2 [35,47,48]. TiO_2 is mainly formed on the surface of nickel-based alloys during high-temperature oxidation with low-oxygen partial pressure conditions [34] in S-CO_2 environments. In some cases, the TiO_2 layer is observed on the top of the chromia [44]. Paradoxically, Cr_2O_3 is supposed to form in the outer layer due to TiO_2 being thermodynamically more stable than Cr_2O_3. This is attributed to the lower metal activity of Ti and the higher diffusion rate of Ti ions outward through the chromium layer, thus this phenomenon is reasonable in both thermodynamics and kinetics [49]. In most situations, however, the TiO_2 layer is under the chromia and is able to resist corrosion.

However, if Ti does not exist as TiO_2, the effect of Ti in corrosion resistance could be adverse. The dissolved Ti will refine the grain of the Cr layer, and the substitution of Cr^{3+} by Ti^{4+} will be compensated by electron or cationic vacancy [25,50]. Both of the behaviours mentioned above will lead to the increase of the cation to diffuse along the grain boundary [51]. This behaviour of Ti will finally affect the corrosion resistance of nickel-based alloys both positively and adversely, which will depend on the composition of the alloys and the environments [48].

3.2.3. Effect of Al Content

Al tends to react with oxygen to form alumina. When the content of Al is sufficient, alumina will act as a barrier to prevent the permeation and penetration of C. When the content of Al is relatively low, the Al-rich phase and the Cr-rich phase will be excessively segregated and will deteriorate corrosion resistance.

As an alloying element, Al usually has a positive effect on the corrosion resistance of nickel-based alloys at high temperatures. Similar to Cr, Al also forms a protective oxide layer [44,48]. The formation of Al_2O_3 can be promoted by $(Cr,Fe)_2O_3$, which acts as a crystal template [44]. The formed Al_2O_3 is thermodynamically more stable than Cr_2O_3, which can prevent C from permeating and penetrating into the matrix [52]. B.A. Pint [51] compared the corrosion behaviour of chromia-forming nickel-based alloys such as Alloy 230, Alloy 282, and Alloy 740 and alumina-forming nickel-based alloys such as Alloy 214 and Alloy 247 up to 750 °C in 20 MPa S-CO_2 for 500 h. Results show that the weight gain rate of alumina-forming alloys decreases at higher temperatures. This can be ascribed to the slow growth rate and selective oxidation of aluminum [53]. In addition, almost no amorphous C or carbide precipitation was observed in Alloy 217, this suggests that Alloy 217 has high carburization resistance as a result of higher Al content.

Al also has an adverse effect on the corrosion resistance of nickel-based alloys. According to Oleksak [44], when the chromia scale is formed, the content of Al will lead to internal oxidation, which is inevitable for Ni–Cr–Al alloys, and thus increase the oxidation rate. Although some researchers suggest that for Ni–Cr–Al alloys the internal oxidation can be beneficial by filling the void created by vacancy injection to improve scaling adhesion [54]. It should still be noted that relatively higher Al content will cause a negative effect on corrosion resistance at low temperatures due to the formation of Cr–Al segregation [55]. However, when the content of Al is high enough, then a continuous alumina layer will form instead of the chromia layer, which will improve the corrosion resistance of the alloy better than chromia.

Moreover, Al can deposit on the surface of the alloy and improve the corrosion resistance of alloy. Ho Jung Lee et al. [56] used PVD and an electron beam surface treatment to form an Al micro-alloying zone. After the surface treatment, a preoxidation operation was performed for some specimens at 900 °C for 20 h in high-purity helium. Then, a corrosion test was conducted for as-received, surface-treated and surface-treated + preoxidation specimens at 600 °C and 20 MPa for 500 h in a S-CO_2 environment. The results of the oxide thickness are shown in Figure 3. Compared with the as-received specimens, the EB surface-treated specimen does not show superior corrosion resistance, while the thickness of the oxide layer has barely increased for the EB surface-treated + preoxidation specimens, which suggests greater corrosion resistance. No amorphous C was observed at the interface between the oxide layer and the matrix for the EB surface-treated + preoxidation specimens as well, which suggests superior carburization resistance. The good corrosion resistance of the EB surface-treated + preoxidation specimens is due to the formation of α-alumina, which is stable after further exposure in S-CO_2.

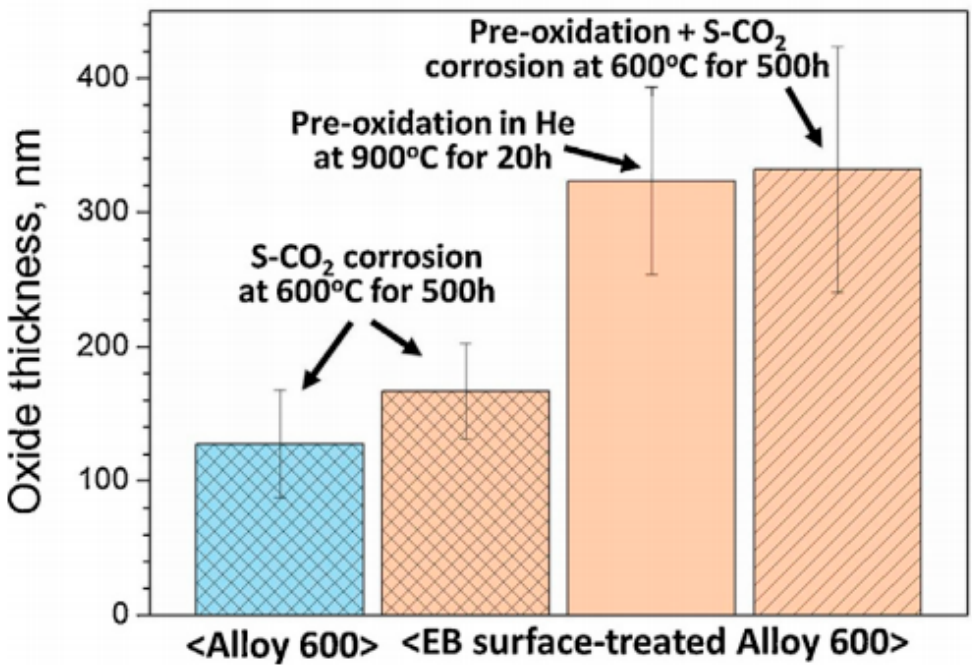

Figure 3. The thickness of oxide layer for the three different experimental conditions. Reprinted from Ho Jung Lee, Sung Hwan Kim, Hyunmyung Kim, and Changheui Jang. "Corrosion and carburization behavior of Al-rich surface layer on Ni-base alloy in supercritical-carbon dioxide environment." Applied Surface Science 388 (2016): 483–490, Copyright 2015, with permission from Elsevier [56].

As a carbide-forming element, the presence of Mo will consume C, which will otherwise react with Cr and prevent the formation of the protective layer. However, excessive content of Mo may lead to the accumulation of Mo carbide and the deterioration of corrosion resistance.

In order to cope with the aggressive environments, Mo is added into the alloy as an alloying element to improve corrosion resistance. Many researchers have observed the formation and precipitation of the Mo carbide [34,57,58], which suggests that Mo is a kind of carbide-forming element. Mo will combine with the C priority to prevent the formation of carbide between Cr and C. This promotes the formation of chromia and increases corrosion resistance. Appropriate content of Mo can improve corrosion resistance, while excessive content of Mo may affect corrosion resistance adversely. For example, the Mo content of Hastelloy-C276 is 17%. The Mo carbide extending from the substrate to the surface was observed [41]. It was found that the Mo carbide could promote the formation of oxide nodules on the surface and break the continuity of the chromia layer, which may decrease the corrosion resistance.

3.2.4. Effect of Si Content

Si has a higher affinity of O than other alloying elements and thus usually presents as silica. If the content of Si is appropriate, it will increase corrosion resistance by preventing bilateral diffusion. However, an excessive content of Si will break the adhesion between the oxide layer and the matrix. Thus, the effect of Si on corrosion resistance is two-sided.

On the positive side, SI can form a thin and continuous silica film layer [48]. SI will act as a barrier to hinder the C to diffuse into the matrix and form carburized regions. The silica can also prevent the outward diffusion of Cr^{3+} to slow the growth rate of chromia [44]. It should be noted that continuous silica can be formed only when the content of Si is sufficient [44]. The critical point of the Si content is 0.3% [58] at 650 °C S-CO_2. However, for the mechanism of Si improving oxidation resistance, some researchers have put forth different opinions. B. Ahmad [59] suggests that the presence of Si can enhance the diffusion

ability of Cr in the alloy, while B. Li [60] believes that the existence of Si promotes the specific chromia to form during the transient phase of oxidation.

On the negative side, excessive content of Si will produce an adverse effect on both corrosion resistance and the mechanical properties of the alloy. Excessive Si content will increase the brittleness of the material and weaken its mechanical properties. In addition, the existence of silica between the oxide layer and the matrix will inevitably affect the adhesion of the oxide layer [61], resulting in spallation. Based on the behaviour of Si, the content of Si is very important for the corrosion-resistant alloy, and a balance should be established between ensuring corrosion resistance and not affecting the mechanical properties of the alloy.

3.2.5. Effect of Mn Content

The effect of Mn depends on the corrosion product. When Mn and Cr react together to form spinel-phase oxides such as $MnCr_2O_4$ and $(Mn,Cr)_3O_4$, they will resist carburization. However, the oxide layer formed by Mn alone is irregular, which will deteriorate corrosion resistance.

Mn intends to form a spinel $MnCr_2O_4$-phase layer with Cr beneath the chromia layer [62] according to some studies [37,42,48,50]. The $MnCr_2O_4$ will act as a barrier to carburization similar to silica. However, studies have shown that Mn will change the diffusion boundary condition [63] and lead to linear reduction of the oxidation rate [44] until the content of Mn reaches 0.45% [64]. If the content of Mn is inappropriate, this will result in the formation of an irregular oxide layer and decrease corrosion resistance. Thus, it is crucial to determine the appropriate Mn content to ensure a positive effect on the corrosion resistance of the alloy.

3.3. Summary

This section mainly summarizes the effect of various alloying elements on the corrosion resistance of nickel-based alloys at high-temperature and -pressure S-CO_2, including the major and trace alloying elements. For major elements, the content of Fe and Ni is associated with the carburization resistance of nickel-based alloys. The content of Cr is the most significant factor for determining the corrosion resistance of nickel-based alloys. For trace elements, it is important to determine their appropriate content in nickel-based alloys to maintain a positive effect and eliminate adverse effects.

4. Parameters Related to the Corrosion Environment

Section 3 mainly described the effect of the content of alloying elements on the corrosion resistance of nickel-based alloys. This section introduces the parameters related to the corrosion environment of nickel-based alloys such as temperature, pressure, impurities and flow rate.

4.1. Effect of Temperature and Pressure

4.1.1. Effect of Temperature

As a promising power conversion system, the S-CO_2 Brayton cycle can be used for solar power, nuclear reactors, thermal power generation and so on. These applications have high requirements for temperature and pressure [63], which will inevitably affect the corrosion behaviour of the structural materials in the S-CO_2. Therefore, temperature and pressure are important factors that must be considered in the process of S-CO_2 corrosion. The effect of temperature is discussed in this section.

Ho Jung Lee et al. [37] tested Alloy 600, Alloy 690 and Alloy 800HT at 550, 600, 650 °C and 20 MPa for 1000 h. As shown in Figure 4, the weight gain and thickness of the oxide layer are quite small, which proves that the alloys have excellent corrosion resistance at these temperatures.

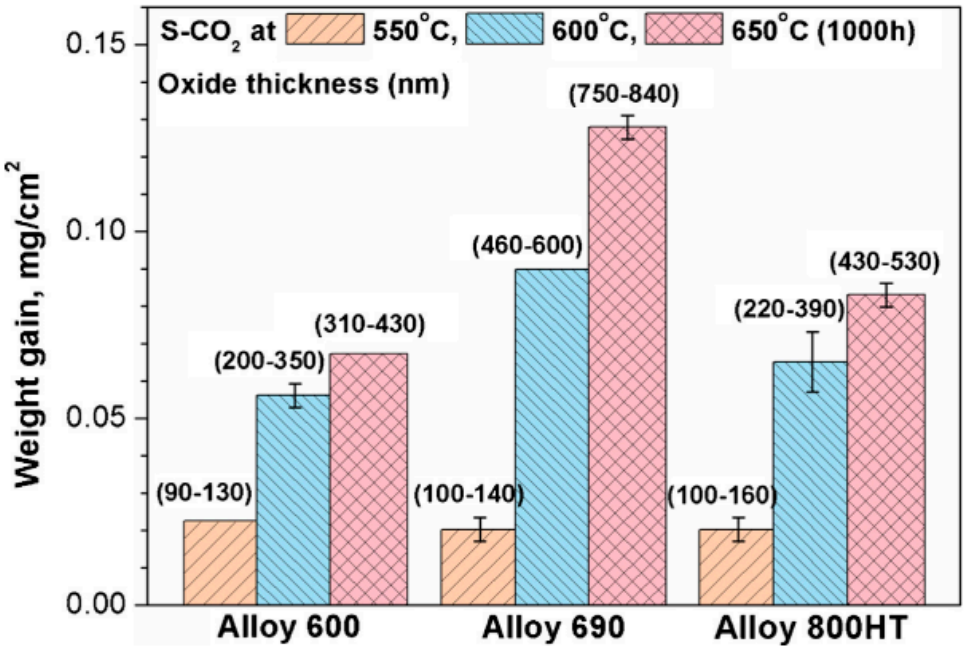

Figure 4. Weight gain and oxide thickness of the tested alloys. Reprinted from Ho Jung Lee, Hyunmyung Kim, Sung Hwan Kim, and Changheui Jang. "Corrosion and carburization behavior of chromia-forming heat resistant alloys in a high-temperature supercritical-carbon dioxide environment." Corrosion Science 99 (2015): 227-239, Copyright 2015, with permission from Elsevier [37].

When the temperature is 550 °C, the difference of oxide thickness between the alloys is small. However, with the increase in temperature, the thickness of the oxide layer was significantly thicker than 550 °C at 600 °C and slightly thicker at 650 °C. Moreover, with the increases in temperature, the oxide composition of the alloys also changed. In addition to Cr_2O_3, the peaks for minor oxides such as $Mn_{1.5}Cr_{1.5}O_4$ and TiO_2 are also observed according to the XRD results. According to Zhongliang Zhu's research [2], the corrosion kinetics are proportional to the weight gain, which suggests that the lower weight gain corresponded to better corrosion resistance. Therefore, the order of corrosion resistance is 550 °C > 600 °C > 650 °C. This is mainly because when the temperature is low, the system cannot provide enough energy for reactions such as diffusion and oxidation [35]. For the higher temperature range, Olivares et al. [62] have done some research. Alloy 282, Alloy 230, Alloy HR160, Alloy HR120 and Alloy 188 were tested at 700–1000 °C, 20 MPa S-CO_2. Their study shows that with the increase in temperature, the weight gain of the alloy has a dramatic increase, while the change in the internal oxidation zone is moderate. They drew the same conclusion that with the increase in temperature, the corrosion of the alloys in S-CO_2 becomes worse.

Furthermore, research on the effect of carburization behaviour has been done as well [37,65]. With the increase in temperature, the structure of the outer oxide layer will change from single layer to double layer [37]. In this process, defects such as pores, cracks and oxide grain boundaries in the chromia layer will be created and thus cause the diffusion of CO or CO_2 [65]. This causes C to permeate and penetrate through the chromia layer even though C is almost insoluble in the oxide [65]. With the temperature increasing, it is reported that the depth of carbide formation increased as well for Alloy 800HT, while the carburization rate of Alloy 600 and Alloy 690 barely changed. This suggests that the increase in temperature affects the diffusion rate of C to form coarser and deeper carbides [66].

Up to now, the test temperature for the corrosion behaviour of nickel-based alloys in S-CO_2 has been in the range of 550–750 °C [37,66]. The corrosion behaviour at higher temperatures has hardly been studied. However, S-CO_2 will become more corrosive at

higher temperatures [67]. Thus, the corrosion behaviour of nickel-based alloys at higher temperatures needs to be investigated more in the future.

4.1.2. Effect of Pressure

Regarding the effect of pressure on corrosion behaviour, there are mainly two kinds of conclusions in the current research. Some researchers suggest that increasing pressure will lead to changes in corrosion behaviour [66,68]. Other researchers believe that external environment pressure has a minor effect on corrosion behaviour [35,51,69–71]. Ho Jung Lee et al. [66] tested Alloy 600, Alloy 690 and Alloy 800HT at 600 °C by increasing the pressure from 0.1 MPa to 20 MPa for 1000 h. The results are shown in Figure 5 and suggest that with the increase in pressure, the alloys show a certain amount of weight gain. This may be induced by enhancement of the inward diffusion of the oxidant through the grain boundaries or defects in the oxide layer under high pressure [66].

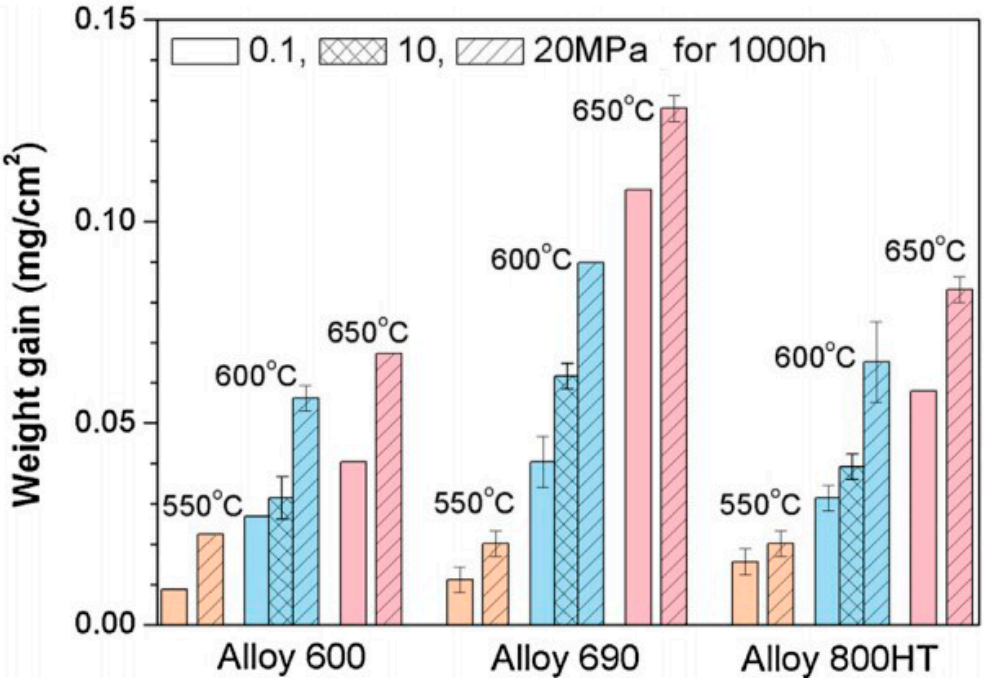

Figure 5. Weight gain of tested alloys in different S-CO_2 environments. Reprinted from Ho Jung Lee, Gokul Obulan Subramanian, Sung Hwan Kim, and Changheui Jang. "Effect of pressure on the corrosion and carburization behavior of chromia-forming heat-resistant alloys in high-temperature carbon dioxide environments." Corrosion Science 111 (2016): 649–658, Copyright 2016, with permission from Elsevier [66].

Other studies [69,70] show an opposite conclusion. For chromia-forming and alumina-forming nickel-based alloys, the weight gain shows minimal change with the increase of pressure. Oleksak et al. [71] tested a few nickel-based alloys and found that the change in pressure would not lead to the change in corrosion behaviour of the alloys.

However, B. A. Pint [68] tested Alloy 625 and found that the increase in pressure may have a positive effect on corrosion resistance. With the pressure increase, Alloy 625 formed a thicker oxide layer with less voids at 750 °C. The oxide layer is denser and more protective than those formed in lower pressure. This may be attributed to the faster oxidation rate under higher pressure, which can reduce the defects of the oxide layer.

Ho Jung Lee's research [66] observed that the amount of accumulated C increased at the interface between the oxide layer and the matrix with the increase of pressure. However, the carburization could not penetrate deeper because the depth was determined by the diffusivity of C in the matrix instead of the ambient pressure.

4.1.3. Summary

In conclusion, temperature has a great effect on S-CO_2 corrosion behaviour. Increasing temperature not only accelerates the molecular thermal motion but also changes the composition of the corrosion product layer. This results in more holes, cracks and other defects and accelerates S-CO_2 corrosion. Compared with temperature, pressure has little effect on the corrosion of S-CO_2. Increasing pressure will lead to enhancement of the oxidation rate and the thickness of oxidation products, thus accelerating corrosion.

4.2. Effect of Impurities

Impurities such as O_2, H_2O, CO and SO_2 will inevitably be added in the corrosion process of S-CO_2 under actual conditions. The impurities will affect the corrosion rate and corrosion products by altering thermodynamic and kinetic conditions [72]. Thus, studies have been made to explore the effect of impurities on corrosion behaviour of nickel-based alloys with two categories of S-CO_2: research grade (RG) and industrial grade (IG). The purity of RG and IG conditions are 99.999% and 99.95%, respectively [49]. This section introduces the effect of various impurity contents on the corrosion behaviour of nickel-based alloys.

4.2.1. Effect of H_2O

As a common impurity, H_2O will be easily added into S-CO_2 corrosive environments in the form of water vapor. According to the studies by [73,74], the existence of H_2O will create more path to diffuse, change the characteristic of diffusion, make water molecular to diffuse into the matrix and vaporize surface oxide [75,76]. This results in the thickening of oxide layer, which can increase the amount of defects and induce spallation.

A study by [74] indicates that for Alloy 740, adding 100 ppm H_2O thickens the oxide layer and increases the number of nodules. However, another study [77] suggests that the alloys do not gain more weight with the addition of H_2O. At present, there is little research on the effect of H_2O as the sole impurity in the corrosion behaviour of nickel-based alloys in high-temperature and -pressure S-CO_2. Therefore, more research should be done to reveal the effects of H_2O.

4.2.2. Effect of O_2

Many studies have been conducted on the effect of O_2 as an impurity on the corrosion behaviour of nickel-based alloys in high-temperature and -pressure S-CO_2. However, the conclusions they have drawn have some distinctions. The corrosion behaviour of Haynes 230 in S-CO_2 with different O_2 contents at 650 and 750 °C was studied [78]. As shown in Figure 6, those groups that contain O_2 show a higher weight gain than the pure RG group, which means corrosion intensification. The explanation is that with the addition of O_2, the rate of Cr diffusion will be accelerated and lead to formation of the oxide layer with more defects. The results of another study [79] indicated that the existence of O_2 led to a thicker oxide layer and higher mass gain.

However, other studies have indicated positive effects of O_2. Alloy 740 formed an oxide layer that is thinner and with fewer defects at 600 °C and 30 MPa with 100 ppm O_2 added [74]. However, the effect of O_2 on carburization was negligible. This can be attributed to the steady oxide layer that is formed by the assistance of O_2 instead of S-CO_2 due to O_2 being thermodynamically more likely to form chromia with Cr.

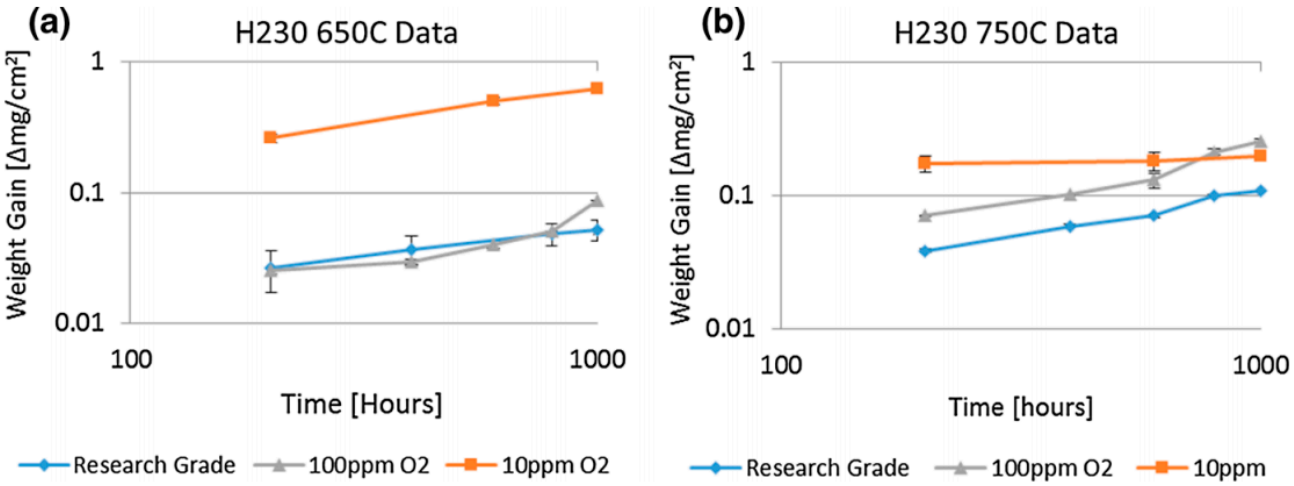

Figure 6. Weight gain of Haynes 230 at different S-CO_2 purity levels at (**a**) 650 °C and (**b**) 750 °C. Reprinted from Jacob Mahaffey, David Adam, Andrew Brittan, Mark Anderson, and Kumar Sridharan. "Corrosion of alloy Haynes 230 in high temperature supercritical carbon dioxide with oxygen impurity additions." Oxidation of Metals 86 (2016): 567–580, Copyright 2016, with permission from Springer Nature [78].

4.2.3. Effect of H_2O + O_2

When both H_2O and O_2 exist in S-CO_2 environments, the oxide layer on the surface of the nickel-based alloy evaporates. This causes the oxide layer to lose protection and continuity, leading to the deterioration of corrosion resistance [73]. The chemical reaction that will occur during this process is shown as Reaction (7) [80,81]:

$$2Cr_2O_3 + 3O_2 + 4H_2O \rightarrow CrO_2(OH)_2 \quad (7)$$

Due to the serious effect on the corrosion resistance of the nickel-based alloy that Reaction (7) will bring, some studies on the synergistic effect of H_2O and O_2 have been conducted [35,49,70]. Oleksak et al. [35] suggest that at high pressure, chromium volatilization will occur with the presence of H_2O + O_2. Several nickel-based alloys have been tested at 750 °C and 30 MPa in S-CO_2 environments with 1% O_2 and 0.25% H_2O [70]. The light microscopy images of cross section for some alloys are shown in Figure 7. It can be obviously seen that the amount of nodules on the surface and the internal oxidation in the matrix increased with the addition of O_2 and H_2O. Lehmusto [49] used the method of isotope labeling. He replaced the O in H_2O with O_{18}. The results show that in S-CO_2 environments with O_2 and H_2O, H_2O molecules do not dominate the reaction but instead induce it due to the disappearance of O^{18} in the oxide layer after exposure.

Nevertheless, there are also some studies that found that the existence of both H_2O and O_2 may improve corrosion resistance [81]. It is suggested that there is a critical point of O_2 content (about 2%). When the content of O_2 is more than 2%, a thermodynamically stable and continuous chromia layer will be formed in S-CO_2 environments [81]. As for H_2O, it tends to support the growth of oxides and induce evaporation of the surface oxide layer, which corresponds to the findings by Lehmusto [49].

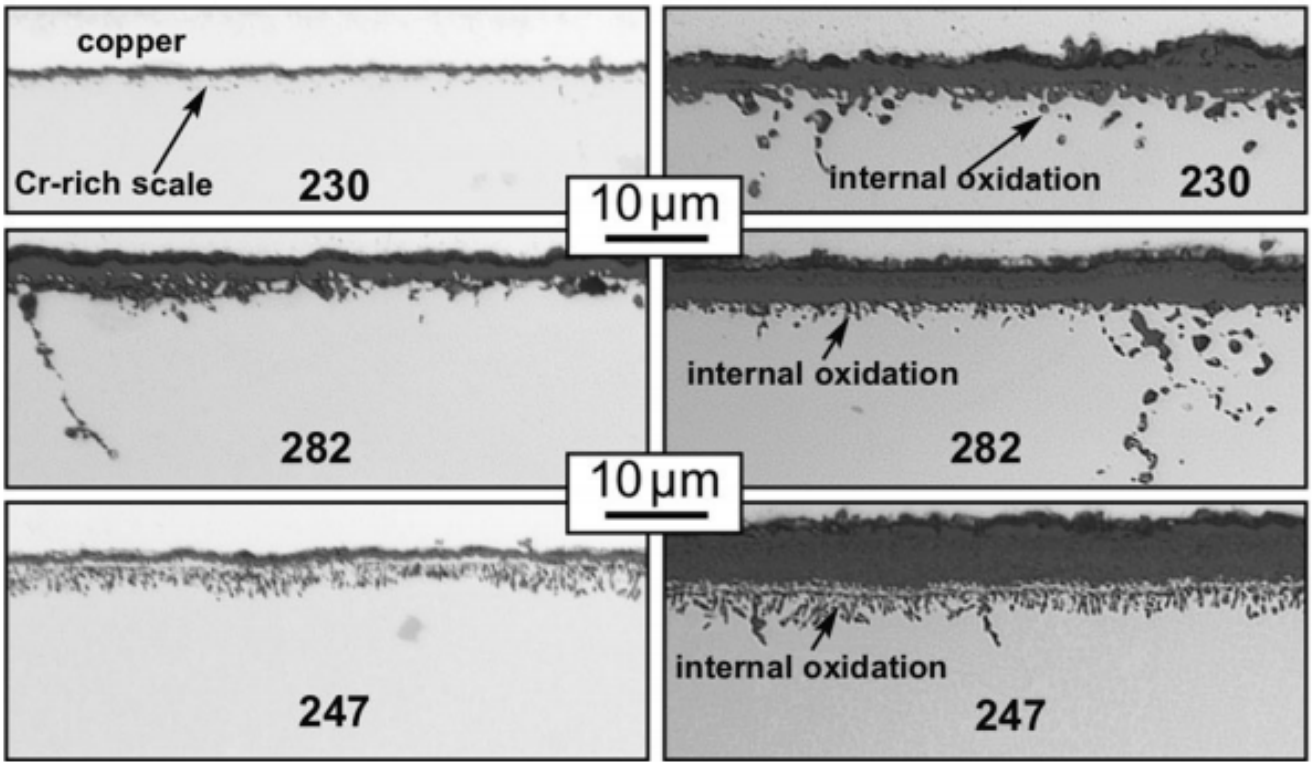

Figure 7. Light microscopy images of cross section at RG S-CO_2 with or without impurities. Reprinted from Pint, Bruce A., Juho Lehmusto, Michael J. Lance, and James R. Keiser. "Effect of pressure and impurities on oxidation in supercritical CO_2." Materials and Corrosion 70, no. 8 (2019): 1400–1409, Copyright 2019, with permission from John Wiley and Sons [70].

4.2.4. Effect of CO

Due to the incomplete combustion of fossil fuels, some CO impurities may be added into S-CO_2. A study [82] suggests that as a reducing gas, the existence of CO will lead to promotion of C deposition on the surface oxide layer. However, when the content of CO exceeds 1%, it will create defects such as voids, holes and cracks and transform the dense surface chromia layer into a porous one. The porous layer facilitates the permeation and diffusion of the corrosive gas into the matrix, leading to deterioration of corrosion resistance. The corrosion behaviour of Alloy 625 has been tested at 750 °C and 20 MPa S-CO_2 with and without 1% CO for 1000 h [82]. The cross-sectional SEM images of the oxide layer that is formed on Alloy 625 is shown in Figure 8. For Alloy 625, a thicker and more porous chromia layer is formed with the presence of 1% CO, which suggests worse corrosion resistance. CO will not be beneficial to the corrosion resistance of the alloys. Thus, for further studies, researchers should put a premium on the elimination of CO from the Brayton cycle.

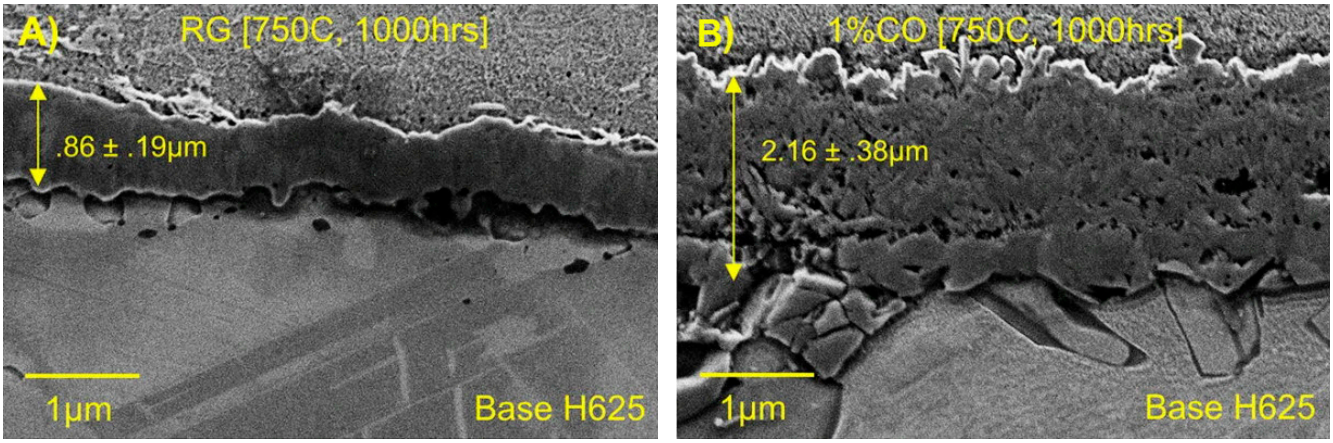

Figure 8. The cross-sectional SEM images of oxide layer (**A**) RG S-CO_2; (**B**) RG S-CO_2 + 1%CO. Reprinted from Jacob Mahaffey, Anthony Schroeder, David Adam, Andrew Brittan, Mark Anderson, Adrien Couet, and Kumar Sridharan. "Effects of CO and O_2 impurities on supercritical CO_2 Corrosion of alloy 625". Metallurgical and Materials Transactions A 49 (2018): 3703–3714, Copyright 2018, with permission from Springer Nature [82].

4.2.5. Effect of SO_2

As an acidic medium, SO_2 will adversely affect the corrosion behaviour of the alloy in S-CO_2 environments. Oleksak et al. [44] have conducted research on the effect of SO_2. SO_2 is highly corrosive even if the pressure is atmospheric. Another study [83] investigated the effect of adding 0.1% SO_2 on the corrosion behaviour of five nickel-based alloys at different temperatures. The results are shown in Figure 9. The results show that with the lower ambient temperature, the corrosiveness of SO_2 becomes more severe. However, the most corroded alloy (Alloy 617) happens to have a relatively high Cr content. This suggests that the corrosiveness of SO_2 is related to the environments and the relationship with the alloy composition needs to further test.

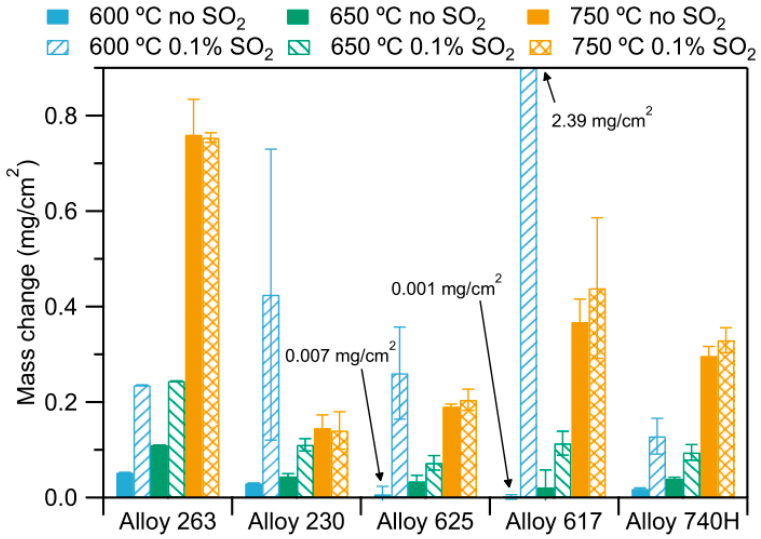

Figure 9. Mass change of five alloys exposed at 600–750 °C for 1500 h to 95% S-CO_2, 4% H_2O and 1% O_2 with or without 0.1% SO_2. Reprinted from Richard P. Oleksak, Joseph H. Tylczak, Gordon R. Holcomb, and Ömer N. Doğan. "Temperature-dependence of corrosion of Ni-based superalloys in hot CO_2-rich gases containing SO_2 impurities." JOM 72, no. 5 (2020): 1822–1829, Copyright 2020, with permission from Springer Nature [83].

4.3. Effect of Flow Rate

As a fluid between the gaseous state and the liquid state, S-CO_2 flows in actual working conditions. Thus, the flow rate of the fluid will affect the corrosion behaviour of the alloy as well. Oleksak [35] believes that at the flow rate of a real S-CO_2 system, chromium volatilization should be considered as a potential problem. The increase of flow rate will generally aggravate local corrosion. There are two reasons for this phenomenon: the fluid flow under dynamic condition promotes the mass transfer process of S-CO_2 to the specimen surface [84] and also promotes the electrochemical reaction of corrosion by changing the local chemical environment [85]. In addition, the flow of S-CO_2 fluid will produce shear stress on the sample surface [86] and destroy the continuity and compactness of the oxide layer on the surface of the alloy. The incomplete oxide layer will aggravate the corrosion. However, due to the obstacles of the experimental equipment still unsolved, the above conclusions are based on previous studies on the effect of S-H_2O flow rate on alloy corrosion behaviour. Therefore, more studies should be done when the problem of equipment is solved.

5. Conclusions and Outlook

Nickel-based alloy is used as an alternative candidate material in the S-CO_2 Brayton cycle system, and its corrosion behaviour is still in the exploratory stage. In view of the research completed so far, the following conclusions are made in this paper, and the problems to be solved are proposed:

- For the corrosion mechanism, the corrosion process of materials in S-CO_2 is mainly controlled by ion diffusion, and the corrosion process is divided into oxidation and carburization. Nickel-based alloys have better corrosion resistance than austenitic stainless steel and ferritic/martensitic steel, because nickel-based alloys can form a dense oxide layer to prevent further corrosion. In addition, the nickel matrix has a lower activity of Cr and lower solubility and diffusivity of C.
- The factors affecting the corrosion behaviour of nickel-based alloys in S-CO_2 environments can be mainly divided into two categories: the content of alloying elements and environmental factors.
- Alloying elements can be divided into major elements and trace elements, and these elements play a decisive role in the corrosion resistance of nickel-based alloy. For major elements, the resistance of the alloy to oxidation and carburization increases with the increase of Ni and Cr content. However, for trace elements, the effect of some elements on the corrosion resistance of the alloy should be analyzed according to the specific situation.
- Temperature is one of the most significant factors that affect alloy corrosion behaviour. Under high-temperature conditions, the corrosion of alloys in S-CO_2 will be aggravated, especially oxidation. However, carburization may reduce with increasing temperature under certain conditions.
- Increases in pressure will increase the oxidation and carburization rate, thus accelerating corrosion. In some cases, a denser layer will also be formed, increasing the corrosion resistance of the alloys.
- The presence of impurities such as O_2, H_2O, CO and SO_2 usually accelerates the corrosion of alloys in S-CO_2. The addition of O_2 (with H_2O) and CO will speed up the oxidation process. The formed oxide layer will thicken, spallation will occur, and the corrosion will be aggravated. As an acidic medium, SO_2 will accelerate the corrosion of alloys as well.
- Compared with the above factors, the flow rate has little effect on the corrosion of alloys in S-CO_2, which mainly changes the chemical environment of the alloy surface, promotes mass transfer and imposes shear stress.

In view of the current research, this paper puts forward the following problems to be solved:

- The working environment of candidate alloys in the Brayton cycle is harsh; thus, stress is likely to exist. The corrosion behaviour of alloys with stress should be considered and studied in the future.
- The effects of some trace alloying elements on the corrosion resistance of the alloy are seldom studied. The corrosion behaviour of these elements in S-CO_2 should be defined.
- Studies on the effect of S-CO_2 flow rate on alloy corrosion behaviour are currently lacking due to obstacles in experimental equipment. Research should be conducted after the problem of experimental equipment is solved.
- The integrity of the corrosion-resistant oxide layer would depend on the effective pinning of the inner layer when the corrosion layers are multiple. Thus, how the inherent impurities of the alloy will affect the pinning phenomenon should be discussed.
- Surface coating, as a nanocrystaline microstructure, is widely used in corrosion protection. However, the effect of Ni-based alloys with nanocrystaline microstructure on S-CO_2 corrosion has not given attention. Further studies should pay attention to this area.

Author Contributions: Conceptualization, H.C. and X.L.; formal analysis, Y.K. and L.Z.; writing—original draft preparation, Y.K., B.B. and X.W.; writing—review and editing, Y.K. and X.L.; supervision, H.C.; funding acquisition, X.L. and H.C. All authors have read and agreed to the published version of the manuscript.

Funding: The authors are grateful for the financial support of the Guangdong Basic and Applied Basic Research Foundation (No. 2021A1515012411), the Support Plan for Core Technology Research and Engineering Verification of Development and Reform Commission of Shenzhen Municipality (No. 202100037), the Characteristic Innovation Project of Guangdong Educational Department (No. 2022KTSCX217) and the Open Project Program of State Key Laboratory of Advanced Welding and Joining (No. AWJ-23Z04).

Data Availability Statement: The data presented in this study are available on request from the corresponding author.

Conflicts of Interest: The authors declare no conflict of interest.

References

1. Tušek, L.; Golob, V.; Knez, Ž. The Effect of Pressure and Temperature on Supercritical CO_2 Dyeing of PET-Dyeing with Mixtures of Dyes. *Int. J. Polym. Mater. Polym. Biomater.* **2000**, *47*, 657–665. [CrossRef]
2. Zhu, Z.; Cheng, Y.; Xiao, B.; Khan, H.I.; Xu, H.; Zhang, N. Corrosion behavior of ferritic and ferritic-martensitic steels in supercritical carbon dioxide. *Energy* **2019**, *175*, 1075–1084. [CrossRef]
3. Pourmehran, O.; Sarafraz, M.; Rahimi-Gorji, M.; Ganji, D. Rheological behaviour of various metal-based nano-fluids between rotating discs: A new insight. *J. Taiwan Inst. Chem. Eng.* **2018**, *88*, 37–48. [CrossRef]
4. Ahn, Y.; Bae, S.J.; Kim, M.; Cho, S.K.; Baik, S.; Lee, J.I.; Cha, J.E. Review of supercritical CO_2 power cycle technology and current status of research and development. *Nucl. Eng. Technol.* **2015**, *47*, 647–661. [CrossRef]
5. Firouzdor, V.; Sridharan, K.; Cao, G.; Anderson, M.; Allen, T. Corrosion of a stainless steel and nickel-based alloys in high temperature supercritical carbon dioxide environment. *Corros. Sci.* **2013**, *69*, 281–291. [CrossRef]
6. Endo, H.; Netchaev, A.; Yoshimura, K.; Arie, K.; Yamadate, M.; Sawada, T.; Ninokata, H. A concept of the multipurpose liquid metallic-fueled fast reactor system (MPFR). *Prog. Nucl. Energy* **2000**, *37*, 291–298. [CrossRef]
7. Xu, J.; Sun, E.; Li, M.; Liu, H.; Zhu, B. Key issues and solution strategies for supercritical carbon dioxide coal fired power plant. *Energy* **2018**, *157*, 227–246. [CrossRef]
8. Cheang, V.; Hedderwick, R.; McGregor, C. Benchmarking supercritical carbon dioxide cycles against steam Rankine cycles for Concentrated Solar Power. *Sol. Energy* **2015**, *113*, 199–211. [CrossRef]
9. Liu, Y.; Wang, Y.; Huang, D. Supercritical CO_2 Brayton cycle: A state-of-the-art review. *Energy* **2019**, *189*, 115900. [CrossRef]
10. Liu, Y.; Wang, Y.; Zhang, Y.; Hu, S. Design and performance analysis of compressed CO_2 energy storage of a solar power tower generation system based on the S-CO_2 Brayton cycle. *Energy Convers. Manag.* **2021**, *249*, 114856. [CrossRef]
11. Xu, C.; Zhang, Q.; Yang, Z.; Li, X.; Xu, G.; Yang, Y. An improved supercritical coal-fired power generation system incorporating a supplementary supercritical CO_2 cycle. *Appl. Energy* **2018**, *231*, 1319–1329. [CrossRef]

12. Sarrade, S.; Féron, D.; Rouillard, F.; Perrin, S.; Robin, R.; Ruiz, J.-C.; Turc, H.-A. Overview on corrosion in supercritical fluids. *J. Supercrit. Fluids* **2017**, *120*, 335–344. [CrossRef]
13. Rouillard, F.; Furukawa, T. Corrosion of 9-12Cr ferritic–martensitic steels in high-temperature CO_2. *Corros. Sci.* **2016**, *105*, 120–132. [CrossRef]
14. Tan, L.; Anderson, M.; Taylor, D.; Allen, T. Corrosion of austenitic and ferritic-martensitic steels exposed to supercritical carbon dioxide. *Corros. Sci.* **2011**, *53*, 3273–3280. [CrossRef]
15. Li, K.; Zhu, Z.; Xiao, B.; Luo, J.-L.; Zhang, N. State of the art overview material degradation in high-temperature supercritical CO_2 environments. *Prog. Mater. Sci.* **2023**, *136*, 101107. [CrossRef]
16. Yang, L.; Qian, H.; Kuang, W. Corrosion Behaviors of Heat-Resisting Alloys in High Temperature Carbon Dioxide. *Materials* **2022**, *15*, 1331. [CrossRef]
17. Jing, J.; Chen, Z.; Feng, C. Using the photoinduced volt-ampere curves to study the p/n types of the corrosion products with semiconducting properties. *J. Electroanal. Chem.* **2021**, *881*, 114961. [CrossRef]
18. Gheno, T.; Monceau, D.; Zhang, J.; Young, D. Carburisation of ferritic Fe–Cr alloys by low carbon activity gases. *Corros. Sci.* **2011**, *53*, 2767–2777. [CrossRef]
19. Gui, Y.; Liang, Z.; Zhao, Q. Corrosion and Carburization Behavior of Heat-Resistant Steels in a High-Temperature Supercritical Carbon Dioxide Environment. *Oxid. Met.* **2019**, *92*, 123–136. [CrossRef]
20. Liang, Z.; Gui, Y.; Zhao, Q. Experimental Study on Corrosion Characteristics of Three Typical Heat-resistant Steels under Supercritical Carbon Dioxide. *J. Xi'an Jiaotong Univ.* **2019**, *53*, 23–29.
21. Liang, Z.; Gui, Y.; Zhao, Q. Study on Corrosion Behaviour and Mechanism of Typical Heat-Resistant STEEL under Supercritical Carbon Dioxide Chinese Academy of Engineering. In Proceedings of the Chinese Society for Corrosion and Protection, Summary Set of the Tenth National Corrosion Conference, Nanchang, China, 24 October 2019. [CrossRef]
22. Yang, H.; Liu, W.; Gong, B.; Jiang, E.; Huang, Y.; Zhang, G.; Zhao, Y. Corrosion behavior of typical structural steels in 500 °C, 600 °C and high pressure supercritical carbon dioxide conditions. *Corros. Sci.* **2021**, *192*, 109801. [CrossRef]
23. Song, L.; Chen, Z.; Hou, B. The role of the photovoltaic effect of γ-FeOOH and β-FeOOH on the corrosion of 09CuPCrNi weathering steel under visible light. *Corros. Sci.* **2015**, *93*, 191–200. [CrossRef]
24. Rouillard, F.; Charton, F.; Moine, G. Corrosion Behavior of Different Metallic Materials in Supercritical Carbon Dioxide at 550 °C and 250 bars. *Corrosion* **2011**, *67*, 095001. [CrossRef]
25. Meier, G.H.; Jung, K.; Mu, N.; Yanar, N.M.; Pettit, F.S.; Abellán, J.P.; Olszewski, T.; Hierro, L.N.; Quadakkers, W.J.; Holcomb, G. Effect of Alloy Composition and Exposure Conditions on the Selective Oxidation Behavior of Ferritic Fe–Cr and Fe–Cr–X Alloys. *Oxid. Met.* **2010**, *74*, 319–340. [CrossRef]
26. Singh, R.; Venkataraman, M.B. High Temperature Corrosion and Oxidation of Metals. *Metals* **2019**, *9*, 942. [CrossRef]
27. Glarborg, P.; Bentzen, L.L.B. Chemical Effects of a High CO_2 Concentration in Oxy-Fuel Combustion of Methane. *Energy Fuels* **2007**, *22*, 291–296. [CrossRef]
28. Cao, G.; Firouzdor, V.; Sridharan, K.; Anderson, M.; Allen, T. Corrosion of austenitic alloys in high temperature supercritical carbon dioxide. *Corros. Sci.* **2012**, *60*, 246–255. [CrossRef]
29. Chen, H.; Kim, S.H.; Kim, C.; Chen, J.; Jang, C. Corrosion behaviors of four stainless steels with similar chromium content in supercritical carbon dioxide environment at 650 °C. *Corros. Sci.* **2019**, *156*, 16–31. [CrossRef]
30. Gui, Y.; Liang, Z.; Shao, H.; Zhao, Q. Corrosion behavior and lifetime prediction of VM12, Sanicro 25 and Inconel 617 in supercritical carbon dioxide at 600 °C. *Corros. Sci.* **2020**, *175*, 108870. [CrossRef]
31. Liang, Z.; Gui, Y.; Wang, Y.; Zhao, Q. Corrosion performance of heat-resisting steels and alloys in supercritical carbon dioxide at 650 °C and 15 MPa. *Energy* **2019**, *175*, 345–352. [CrossRef]
32. Teeter, L.; Adam, B.; Wood, T.; Tucker, J. Comparison of the corrosion of materials in supercritical carbon dioxide, air, and argon environments. *Corros. Sci.* **2021**, *192*, 109752. [CrossRef]
33. Pint, B.A.; Pillai, R.; Lance, M.J.; Keiser, J.R. Effect of Pressure and Thermal Cycling on Long-Term Oxidation in CO_2 and Supercritical CO_2. *Oxid. Met.* **2020**, *94*, 505–526. [CrossRef]
34. Kim, D.; Kim, D.; Lee, H.J.; Jang, C.; Yoon, D.J. Corrosion characteristics of Ni-base superalloys in high temperature steam with and without hydrogen. *J. Nucl. Mater.* **2013**, *441*, 612–622. [CrossRef]
35. Oleksak, R.P.; Holcomb, G.R.; Carney, C.S.; Doğan, Ö.N. Carburization susceptibility of chromia-forming alloys in high-temperature CO_2. *Corros. Sci.* **2022**, *206*, 110488. [CrossRef]
36. Adam, B.; Teeter, L.; Mahaffey, J.; Anderson, M.; Árnadóttir, L.; Tucker, J.D. Effects of Corrosion in Supercritical CO_2 on the Microstructural Evolution in 800H Alloy. *Oxid. Met.* **2018**, *90*, 453–468. [CrossRef]
37. Lee, H.J.; Kim, H.; Kim, S.H.; Jang, C. Corrosion and carburization behavior of chromia-forming heat resistant alloys in a high-temperature supercritical-carbon dioxide environment. *Corros. Sci.* **2015**, *99*, 227–239. [CrossRef]
38. Oleksak, R.P.; Carney, C.S.; Holcomb, G.R.; Doğan, Ö.N. Structural Evolution of a Ni Alloy Surface During High-Temperature Oxidation. *Oxid. Met.* **2018**, *90*, 27–42. [CrossRef]
39. Oleksak, R.P.; Addou, R.; Gwalani, B.; Baltrus, J.P.; Liu, T.; Diulus, J.T.; Devaraj, A.; Herman, G.S.; Doğan, Ö.N. Molecular-scale investigation of the oxidation behavior of chromia-forming alloys in high-temperature CO_2. *Npj Mater. Degrad.* **2021**, *5*, 46. [CrossRef]

40. Rouillard, F.; Moine, G.; Tabarant, M.; Ruiz, J.C. Corrosion of 9Cr Steel in CO_2 at Intermediate Temperature II: Mechanism of Carburization. *Oxid. Met.* **2012**, *77*, 57–70. [CrossRef]
41. Olivares, R.I.; Young, D.J.; Marvig, P.; Stein, W. Alloys SS316 and Hastelloy-C276 in Supercritical CO_2 at High Temperature. *Oxid. Met.* **2015**, *84*, 585–606. [CrossRef]
42. Guo, X.; Liu, Z.; Li, L.; Cheng, J.; Su, H.; Zhang, L. Revealing the long-term oxidation and carburization mechanism of 310S SS and Alloy 800H exposed to supercritical carbon dioxide. *Mater. Charact.* **2022**, *183*, 111603. [CrossRef]
43. Subramanian, G.O.; Lee, H.J.; Kim, S.H.; Jang, C. Corrosion and Carburization Behaviour of Ni-xCr Binary Alloys in a High-Temperature Supercritical-Carbon Dioxide Environment. *Oxid. Met.* **2018**, *89*, 683–697. [CrossRef]
44. Oleksak, R.P.; Tylczak, J.H.; Holcomb, G.R.; Doğan, Ö.N. High temperature oxidation of Ni alloys in CO2 containing impurities. *Corros. Sci.* **2019**, *157*, 20–30. [CrossRef]
45. Davis, J.R. *Nickel, Cobalt, and Their Alloys*; ASM International: Almere, The Netherlands, 2000.
46. Subramanian, G.O.; Kim, S.H.; Chen, J.; Jang, C. Supercritical-CO_2 corrosion behavior of alumina- and chromia-forming heat resistant alloys with Ti. *Corros. Sci.* **2021**, *188*, 109531. [CrossRef]
47. Liang, Z.; Yu, M.; Gui, Y.; Zhao, Q. Corrosion Behavior of Heat-Resistant Materials in High-Temperature Carbon Dioxide Environment. *Jom* **2018**, *70*, 1464–1470. [CrossRef]
48. Zhang, G.; Jiang, E.; Liu, W.; Yang, H.; Wu, Y.; Huang, Y. Compatibility of Different Commercial Alloys in High-Temperature, Supercritical Carbon Dioxide. *Materials* **2022**, *15*, 4456. [CrossRef]
49. Lehmusto, J.; Ievlev, A.V.; Cakmak, E.; Keiser, J.R.; Pint, B.A. A Tracer Study on sCO_2 Corrosion with Multiple Oxygen-Bearing Impurities. *Oxid. Met.* **2021**, *96*, 571–587. [CrossRef]
50. Naoumidis, A.; Schulze, H.; Jungen, W.; Lersch, P. Phase studies in the chromium-manganese-titanium oxide system at different oxygen partial pressures. *J. Eur. Ceram. Soc.* **1991**, *7*, 55–63. [CrossRef]
51. Pint, B.A.; Keiser, J.R. Initial Assessment of Ni-Base Alloy Performance in 0.1 MPa and Supercritical CO_2. *Jom* **2015**, *67*, 2615–2620. [CrossRef]
52. McCarroll, I.; La Fontaine, A.; Nguyen, T.; Smith, A.; Zhang, J.; Young, D.; Cairney, J. Performance of an FeCrAl alloy in a high-temperature CO_2 environment. *Corros. Sci.* **2018**, *139*, 267–274. [CrossRef]
53. Pint, B.A.; Keiser, J.R. The effect of temperature on the sCO2 compatibility of conventional structural alloys. In Proceedings of the 4th International Symposium-Supercritical CO_2 Power Cycles, Pittsburgh, PA, USA, 9–10 September 2014; pp. 1–13.
54. Oleksak, R.P.; Carney, C.S.; Doğan, Ö.N. Effect of pressure on high-temperature oxidation of Ni alloys in supercritical CO_2 containing impurities. *Corros. Sci.* **2023**, *215*, 111055. [CrossRef]
55. Costa, G.; Garg, A.; Brady, M.P. Corrosion of alumina-forming austenitic alloys under the supercritical carbon dioxide-based venus atmospheric surface conditions. *Corros. Sci.* **2023**, *211*, 110882. [CrossRef]
56. Lee, H.J.; Kim, S.H.; Kim, H.; Jang, C. Corrosion and carburization behavior of Al-rich surface layer on Ni-base alloy in supercritical-carbon dioxide environment. *Appl. Surf. Sci.* **2016**, *388*, 483–490. [CrossRef]
57. Rouillard, F.; Moine, G.; Martinelli, L.; Ruiz, J.C. Corrosion of 9Cr Steel in CO_2 at Intermediate Temperature I: Mechanism of Void-Induced Duplex Oxide Formation. *Oxid. Met.* **2012**, *77*, 27–55. [CrossRef]
58. Furukawa, T.; Inagaki, Y.; Aritomi, M. Compatibility of FBR structural materials with supercritical carbon dioxide. *Prog. Nucl. Energy* **2011**, *53*, 1050–1055. [CrossRef]
59. Ahmad, B.; Fox, P. STEM Analysis of the Transient Oxidation of a Ni-20Cr Alloy at High Temperature. *Oxid. Met.* **1999**, *52*, 113–138. [CrossRef]
60. Li, B.; Gleeson, B. Effects of Silicon on the Oxidation Behavior of Ni-Base Chromia-Forming Alloys. *Oxid. Met.* **2006**, *65*, 101–122. [CrossRef]
61. Bates, H.G.A. The Corrosion Behavior of High-Temperature Alloys During Exposure for Times up to 10,000 h in Prototype Nuclear Process Helium at 700 to 900 °C. *Nucl. Technol.* **1984**, *66*, 415–428. [CrossRef]
62. Olivares, R.I.; Young, D.J.; Nguyen, T.D.; Marvig, P. Resistance of High-Nickel, Heat-Resisting Alloys to Air and to Supercritical CO_2 at High Temperatures. *Oxid. Met.* **2018**, *90*, 1–25. [CrossRef]
63. Niewolak, L.; Young, D.; Hattendorf, H.; Singheiser, L.; Quadakkers, W.J. Mechanisms of Oxide Scale Formation on Ferritic Interconnect Steel in Simulated Low and High pO_2 Service Environments of Solid Oxide Fuel Cells. *Oxid. Met.* **2014**, *82*, 123–143. [CrossRef]
64. Nguyen, T.D.; Zhang, J.; Young, D.J. Effects of cerium and manganese on corrosion of Fe–Cr and Fe–Cr–Ni alloys in Ar–20CO_2 gas at 818 °C. *Corros. Sci.* **2013**, *76*, 231–242. [CrossRef]
65. Young, D.J.; Nguyen, T.D.; Felfer, P.; Zhang, J.; Cairney, J.M. Penetration of protective chromia scales by carbon. *Scr. Mater.* **2014**, *77*, 29–32. [CrossRef]
66. Lee, H.J.; Subramanian, G.O.; Kim, S.H.; Jang, C. Effect of pressure on the corrosion and carburization behavior of chromia-forming heat-resistant alloys in high-temperature carbon dioxide environments. *Corros. Sci.* **2016**, *111*, 649–658. [CrossRef]
67. Pint, B.A.; Keiser, J.R. Exploring Material Solutions for Supercritical CO2 Applications above 800 °C. *Oxid. Met.* **2022**, *98*, 545–559. [CrossRef]
68. Pint, B.A.; Unocic, K.A. The Effect of CO_2 Pressure on Chromia Scale Microstructure at 750 °C. *Jom* **2018**, *70*, 1511–1519. [CrossRef]
69. Pint, B.; Brese, R.; Keiser, J. Effect of pressure on supercritical CO_2 compatibility of structural alloys at 750 °C. *Mater. Corros.* **2017**, *68*, 151–158. [CrossRef]

70. Pint, B.A.; Lehmusto, J.; Lance, M.J.; Keiser, J.R. Effect of pressure and impurities on oxidation in supercritical CO_2. *Mater. Corros.* **2019**, *70*, 1400–1409. [CrossRef]
71. Oleksak, R.P.; Tylczak, J.H.; Carney, C.S.; Holcomb, G.R.; Doğan, Ö.N. High-Temperature Oxidation of Commercial Alloys in Supercritical CO_2 and Related Power Cycle Environments. *Jom* **2018**, *70*, 1527–1534. [CrossRef]
72. Zhu, Z.; Li, R.; Liu, X.; Khan, H.I.; Xu, H.; Zhang, N. The characterization of oxide scales formed on ferritic-martensitic steel in supercritical water with dissolved oxygen. *Corros. Sci.* **2020**, *174*, 108810. [CrossRef]
73. Saunders, S.; Monteiro, M.; Rizzo, F. The oxidation behaviour of metals and alloys at high temperatures in atmospheres containing water vapour: A review. *Prog. Mater. Sci.* **2008**, *53*, 775–837. [CrossRef]
74. Li, K.; Zeng, Y.; Luo, J.-L. Corrosion of SS310 and Alloy 740 in high temperature supercritical CO_2 with impurities H_2O and O_2. *Corros. Sci.* **2021**, *184*, 109350. [CrossRef]
75. Essuman, E.; Meier, G.; Żurek, J.; Hänsel, M.; Singheiser, L.; Quadakkers, W. Enhanced internal oxidation as trigger for breakaway oxidation of Fe–Cr alloys in gases containing water vapor. *Scr. Mater.* **2007**, *57*, 845–848. [CrossRef]
76. Young, D.J.; Pint, B. Chromium Volatilization Rates from Cr_2O_3 Scales into Flowing Gases Containing Water Vapor. *Oxid. Met.* **2006**, *66*, 137–153. [CrossRef]
77. Pint, B.A.; Thomson, J.K. Effect of oxy-firing on corrosion rates at 600–650 °C. *Mater. Corros.* **2014**, *65*, 132–140. [CrossRef]
78. Mahaffey, J.; Adam, D.; Brittan, A.; Anderson, M.; Sridharan, K. Corrosion of Alloy Haynes 230 in High Temperature Supercritical Carbon Dioxide with Oxygen Impurity Additions. *Oxid. Met.* **2016**, *86*, 567–580. [CrossRef]
79. Lehmusto, J.; Kurley, J.M.; Lance, M.J.; Keiser, J.R.; Pint, B.A. The Impact of Impurities on Alloy Behavior in Supercritical CO_2 at 700 °C. *Oxid. Met.* **2020**, *94*, 95–111. [CrossRef]
80. Zhang, N.; Cao, Q.; Gui, J.; Li, M.; Ni, Y.; Xu, H. Oxidation and chromia evaporation of austenitic steel TP347HFG in supercritical water. *Mater. High Temp.* **2018**, *35*, 461–468. [CrossRef]
81. Li, K.; Zeng, Y.; Luo, J.-L. Corrosion performance of candidate boiler tube alloys under advanced pressurized oxy-fuel combustion conditions. *Energy* **2021**, *215*, 119178. [CrossRef]
82. Mahaffey, J.; Schroeder, A.; Adam, D.; Brittan, A.; Anderson, M.; Couet, A.; Sridharan, K. Effects of CO and O_2 Impurities on Supercritical CO_2 Corrosion of Alloy 625. *Met. Mater. Trans. A* **2018**, *49*, 3703–3714. [CrossRef]
83. Oleksak, R.P.; Tylczak, J.H.; Holcomb, G.R.; Doğan, N. Temperature-Dependence of Corrosion of Ni-Based Superalloys in Hot CO_2-Rich Gases Containing SO_2 Impurities. *Jom* **2020**, *72*, 1822–1829. [CrossRef]
84. Zhang, N.-Q.; Zhu, Z.-L.; Xu, H.; Mao, X.-P.; Li, J. Oxidation of ferritic and ferritic–martensitic steels in flowing and static supercritical water. *Corros. Sci.* **2016**, *103*, 124–131. [CrossRef]
85. Liu, C.; Shen, T.; Yao, C.; Chang, H.; Wei, K.; Niu, L.; Ma, Z.; Wang, Z. Corrosion behavior of ferritic–martensitic steels SIMP and T91 in fast-flowing steam. *Corros. Sci.* **2021**, *187*, 109474. [CrossRef]
86. Yang, J.; Wang, S.; Wang, J.; Tang, X. Effect of high flow velocity on corrosion behavior of Ni based and Ni-Fe based alloys in supercritical water oxidation environment. *J. Supercrit. Fluids* **2021**, *170*, 105126. [CrossRef]

Disclaimer/Publisher's Note: The statements, opinions and data contained in all publications are solely those of the individual author(s) and contributor(s) and not of MDPI and/or the editor(s). MDPI and/or the editor(s) disclaim responsibility for any injury to people or property resulting from any ideas, methods, instructions or products referred to in the content.